

Analysis of the Modulation Transfer Function Spectral Variation in Different Detector Arrays by Means of Speckle Patterns

Alicia Fernández-Oliveras, Antonio M. Pozo and Manuel Rubiño

Departamento de Óptica, Facultad de Ciencias Universidad de Granada Edificio Mecenaz,
Campus Fuentenueva s/n. 18071 Granada, Spain

E-mail: alilia@ugr.es

Abstract. Today, CCD and CMOS detector arrays present excellent features in imaging systems. To investigate the suitability of each technology according to various applications, in this work we have comparatively studied the quality of the images provided by different cameras. To this end we have used the speckle method to determine the modulation transfer function (MTF) at different wavelengths of the visible spectrum for the detectors of a low-cost CCD video camera and of two scientific cameras (CCD and CMOS). For both the low-cost CCD and the scientific CMOS detectors, the differences between the MTF curves intensify as the spatial frequency augments, while the MTF decreases as the wavelength increases. For the scientific CCD detector, the MTF spectral behavior does not show this trend, and the differences between the MTF curves corresponding to extreme wavelengths are not expected to be significant, as opposed to what appears for the scientific CMOS detector. © 2009 Society for Imaging Science and Technology. [DOI: 10.2352/J.ImagingSci.Technol.2009.53.3.031101]

INTRODUCTION

Cameras with imaging devices based on CCD and CMOS detector matrices¹ are being used more and more in such disparate scientific and technological fields as colorimetry, illumination, and astrophysics. Currently, both types of devices offer excellent features in imaging systems when they are appropriately designed. The consensus is that the two technologies complement each other and will coexist in the future, depending on the application involved.^{2–6} Therefore, to investigate the suitability of the use of one or the other technology according to the specific application of the camera, the complete characterization of the different types of detector matrices becomes necessary.

A system is optically characterized by the modulation transfer function (MTF), the determination of which enables the image produced by the system to be evaluated from its response in spatial frequency.^{7,8} For measuring the MTF of solid-state cameras, the literature cites different methods that differ essentially in the type of target or pattern used as the object. Thus, for example, methods use bar targets,⁹ random targets,^{10,11} canted self-imaging targets,¹² and interferometric fringes.^{13,14}

One of the methods to measure the MTF, established in our laboratory, is based on using a laser speckle pattern as the object.^{15–20} This method is suitable for analyzing the detector independently of the camera lens, given that it does not require a lens to project the pattern. Furthermore, using a tunable laser source, we can characterize the device at different wavelengths, this proving indispensable in multispectral and color-measuring applications.

Speckle is an interference phenomenon that occurs when coherent radiation is scattered from a rough surface. Several techniques can be used to generate the speckle pattern, such as different types of transmissive diffusers (ground glass,¹⁵ fused silica,¹⁶ microlens arrays¹⁷) or integrating spheres.^{18–20}

In the latter case, an aperture situated in front of the integrating sphere enables us to specify the spatial frequency content of the speckle pattern. Two of the apertures used to date are the single-slit¹⁸ and double-slit,¹⁹ both of which present advantages and drawbacks.²⁰ In this work, we have used a single slit situated at the exit port of an integrating sphere.

It bears noting that in the works cited above, the systems analyzed are based generally on scientific CCD cameras, and comparisons were not made between devices of different quality or technology, nor was the MTF spectral variation studied.

The aim of the present work is to apply the optical detector-characterization method, based on the measurement of the MTF with speckle patterns, to the analysis at different wavelengths of the image quality provided by different cameras. Accordingly we have comparatively studied the resulting MTF curves at different wavelengths of the visible spectrum, for the detectors of a low-cost CCD video camera and of two scientific cameras (CCD and CMOS).

High-end scientific cameras have a digital output and are usually based on detector arrays in which pixel pitches between the horizontal and the vertical directions are equal. In general, these kinds of cameras fulfill the following requirements: low noise, high responsivity, large dynamic range, and high resolution. Array linearity and analog-to-digital converter linearity are also important in such cameras.¹

Received Aug. 8, 2008; accepted for publication Jan. 23, 2009; published online Apr. 17, 2009.

1062-3701/2009/53(3)/031101/6/\$20.00.

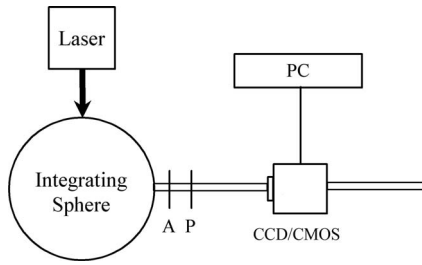


Figure 1. Experimental setup for the measurement of the MTF of the detectors. The aperture A (single slit) and the polarizer P are situated at the exit port of the integrating sphere.

THEORETICAL BACKGROUND

The relationship between the theoretic power-spectral density known for a single slit ($\text{PSD}_{\text{input}}$) and the measured power-spectral density ($\text{PSD}_{\text{output}}$) allows us to determine the MTF of the detector by means of the expression¹⁸

$$\text{PSD}_{\text{output}}(\xi, \eta) = [\text{MTF}(\xi, \eta)]^2 \text{PSD}_{\text{input}}(\xi, \eta), \quad (1)$$

where ξ and η are the spatial frequencies corresponding to the horizontal and vertical directions x and y , respectively.

$\text{PSD}_{\text{output}}$ is determined from the speckle pattern captured with the detector, being proportional to the squared magnitude of the Fourier transform of this speckle pattern. In the case of a rectangular single slit, $\text{PSD}_{\text{input}}$ is given by^{21,22}

$$\text{PSD}_{\text{input}}(\xi, \eta) = \langle I \rangle^2 \left[\delta(\xi, \eta) + \frac{(\lambda z)^2}{l_1 l_2} \text{tri}\left(\frac{\lambda z}{l_1} \xi\right) \text{tri}\left(\frac{\lambda z}{l_2} \eta\right) \right], \quad (2)$$

where $\text{tri}(X) = 1 - |X|$ for $|X| \leq 1$ and zero elsewhere; $\langle I \rangle^2$ is the square of the average speckle irradiance; $\delta(\xi, \eta)$ is a delta function; l_1 and l_2 are, respectively, horizontal and vertical dimensions of the single slit; λ is the wavelength of the laser; and z is the distance between the single-slit aperture and the detector.

Given the geometry of the single slit, the $\text{PSD}_{\text{input}}$ can be separated into frequencies ξ and η . The horizontal $\text{PSD}_{\text{input}}(\xi, \eta)$ is the $\eta=0$ profile of $\text{PSD}_{\text{input}}(\xi, \eta)$, which means that the MTF can be determined separately for x and y directions. In the present work, we determine the horizontal MTF. The same thing can be done for the vertical direction.

METHOD

Experimental Setup

Figure 1 presents the experimental setup used. It is composed of a tunable argon-ion laser source (130 mW) or a He-Ne laser source ($\lambda = 632.8$ nm; 17 mW), depending on the wavelength which is being studied, an integrating sphere to generate the speckle pattern (inner diameter of 152.4 mm), a polarizer to provide a linearly polarized laser-speckle pattern, a single slit (6 mm height and variable

width), and an optical bench to hold the detector, which is connected to the control card installed in a personal computer.

The laser radiation is aimed at the entrance port of the integrating sphere, generating the speckle pattern at the exit port. The aperture situated at the exit port of the sphere (single slit) determines the content in spatial frequency of the pattern registered in the detector. Under these conditions, the linear polarizer ensures that the $\text{PSD}_{\text{input}}$ is given by Eq. (2).²²

With the single slit, the MTF can be determined from a single measurement without the need to move the detector, but it must be situated at a distance from the aperture in such a way that the maximum input spatial frequency is equal to the Nyquist frequency of the detector.^{16,18} In this way, the MTF can be determined over the largest possible frequency range, and thus aliasing is avoided.

The distance z between the detector and the single-slit aperture can be calculated by the expression

$$z = \frac{l_1}{\lambda \xi_{\text{Ny}}}, \quad (3)$$

where l_1 is the slit width, λ the wavelength of the laser, ξ_{Ny} is the Nyquist spatial frequency of the detector in the horizontal direction. For a detector array with a center-to-center spacing between the photoelements Δx , the Nyquist frequency is given by

$$\xi_{\text{Ny}} = \frac{1}{2\Delta x}. \quad (4)$$

In this work, measurements were made using the detectors of three different cameras: a low-cost CCD video camera and two scientific cameras (CCD and CMOS).

The video camera was a CCD B/W Center HICB347H, connected to a Pinnacle Studio™ MovieBox DV control card. Its detector array is comprised of a matrix of 752×582 pixels (horizontal \times vertical). The horizontal spacing between centers of these pixels is $7.98 \mu\text{m}$, providing a Nyquist frequency of 62.66 cycles/mm in the horizontal direction by virtue of Eq. (4).

The scientific CCD camera had a high-resolution CCD B/W PixelFly array of 1360×1024 pixels with a center-to-center spacing between them of $4.65 \mu\text{m}$. Consequently, with Eq. (4) taken into account, the Nyquist frequency of this detector is 107.53 cycles/mm in both directions.

The CMOS camera used was a CMOS B/W Atmos™ Areascan 1M30, the detector array of which had 1312×1024 pixels. In this case the pixel pitch was $5 \mu\text{m}$ in the horizontal as well as in the vertical direction, corresponding to a Nyquist frequency of 100 cycles/mm given by Eq. (4).

The width of the single slit used was $l_1 = 1$ mm in the case of the low-cost video camera CCD detector, and $l_1 = 3$ mm for the two scientific detectors (CCD and CMOS).

Taking into account the width of the single slit and Nyquist frequencies, we can calculate the distance z between

Table I. Distances (mm) between the single-slit aperture and the detector for the three cameras analyzed.

Wavelength (nm)	Low-cost CCD video camera	Scientific CCD camera	Scientific CMOS camera
632.8	25	44	47
514	31	54	58
502	32	—	—
488	33	57	61
477	33	—	—
457	—	61	66
454	35	—	—

the detector and the aperture by using Eq. (3) for each wavelength studied. The corresponding values are listed in Table I for each detector analyzed.

In general, when the speckle method is used with a single slit, setting the accurate distance between the aperture and the detector is problematic because a window is usually placed in front of the sensitive matrix of the detector at an unknown distance. For this reason, in practice, the appropriate position of the detector is set following an experimental procedure. The influence of the systematic error committed setting the detector-aperture distance by this experimental procedure is investigated elsewhere.¹⁵ Thus, the theoretical values of the distance shown above worked as helpful references in fixing the detector-aperture relative position suitable for the measurements.

Data Processing

Once the detector was set at the corresponding distance from the single-slit aperture, as indicated in the previous section, the $\text{PSD}_{\text{output}}(\xi)$ was determined in the following way.

For a given digitized frame of speckle data, a region of 500×500 pixels was selected. Each horizontal row of data is a single observation of an ergodic random process. A fast Fourier transform (FFT), which is a discrete Fourier transform, was performed on each row of speckle data. The magnitude squared in one dimension provided a single estimate of the one-dimensional power spectrum, $\text{PSD}_{\text{output}}(\xi)$. These 500 spectra were averaged, for a better signal-to-noise ratio in the $\text{PSD}_{\text{output}}(\xi)$.²³ To reduce the noise even further, the average was taken for ten frames.

The frames were stored in tiff format without compression, using an integration time of 0.050 s for the scientific CCD detector and 0.004 s for the CMOS detector. In the case of the video camera CCD detector, the frames were extracted in tiff format from a video recording captured at a rate of 25 frames/s for 1 s.

When a FFT is performed on a dataset of length N , the Nyquist frequency appears at the $N/2$ component of the FFT output. A ratio can be formed to evaluate the spatial frequency ξ_n that corresponds to the n th component as²⁰

$$\frac{\xi_{Ny}}{N/2} = \frac{\xi_n}{n} \quad (5)$$

Equation (5) associates frequencies between zero and the Nyquist frequency with FFT components from 0 to the $N/2$ component. In this work, we used $N=1024$, thus the total number of spatial frequencies contained in the range from 0 to the Nyquist frequency of the detector was 512.

Before processing, each digitized frame of speckle data was corrected in order to reduce effects from the spatial noise of the detector itself. With respect to the spatial noise of a CCD, a distinction can be made between the fixed pattern noise (FPN) and the photoresponse nonuniformity (PRNU). The FPN refers to the pixel-to-pixel variation that occurs when the array is in the dark, and thus it is signal-independent noise. The PRNU is due to the difference in response of each pixel to a given signal; it is therefore signal-dependent noise. The FPN was corrected by subtracting from the speckle image the dark image captured by obscuring the detector and the PRNU, by means of the procedure proposed elsewhere.¹⁵

For the processing of the speckle images, the appropriate software was developed using MATLAB®.

RESULTS AND DISCUSSION

For each wavelength analyzed, the experimental values of the horizontal MTF of the detectors were calculated using Eq. (1). For the three detectors, at each wavelength analyzed, a polynomial fit of the experimental MTF values was made, and the resulting functional expression was normalized by dividing it by the value that the adjustment equation provided at zero frequency. The MTF experimental values of the detectors were normalized by dividing them by the same value used to normalize the corresponding adjustment curve (zero-order coefficient in the polynomial-fit expression).

In the case of the video camera CCD detector, six wavelengths were analyzed, five of them provided by the tunable argon-ion laser. For both scientific detector arrays, the total number of analyzed wavelengths was four, and three of them were chosen among those provided by the tunable laser. The choice of these wavelengths was based on preliminary measurements that showed that the number of wavelengths and the separations between them were suitable to analyze the spectral variation of the MTF of each detector.

For both scientific detectors, with the shortest wavelength provided by the tunable laser (454 nm), the signal was an extremely low due to the corresponding values of the slit-detector distance together with the low power of the laser emission for this wavelength. Hence, the lowest wavelength used for the analysis of the CCD and the CMOS scientific arrays was 457 nm instead of 454 nm, as utilized in the study of the video camera CCD detector.

The results are shown in Figures 2–4, which reflect, for the different wavelengths of the visible spectrum, the experimental values of the horizontal MTF of each detector after normalization at zero spatial frequency. For greater clarity,

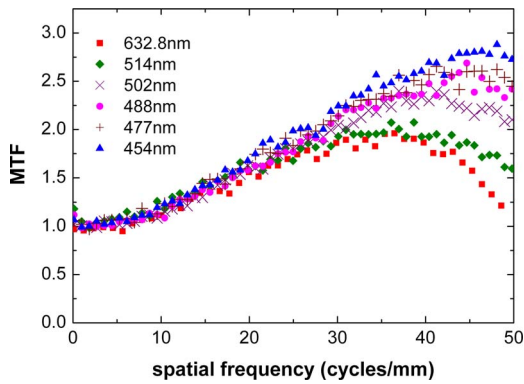


Figure 2. MTF experimental values of the low-cost video camera CCD detector at different wavelengths of the visible spectrum.

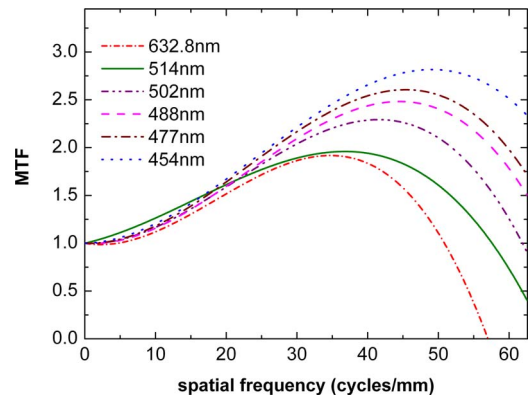


Figure 5. MTF of the low-cost video camera CCD detector at different wavelengths of the visible spectrum. Curves were determined by fitting experimental values to a third-order polynomial function.

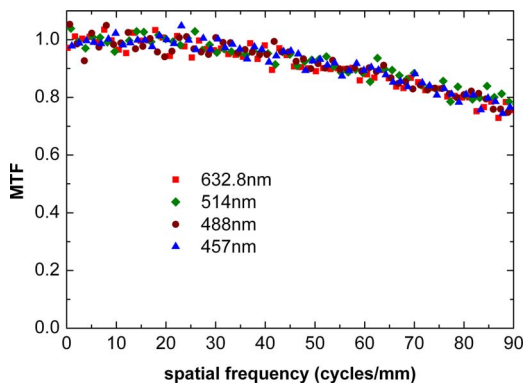


Figure 3. MTF experimental values of the scientific camera CCD detector at different wavelengths of the visible spectrum.

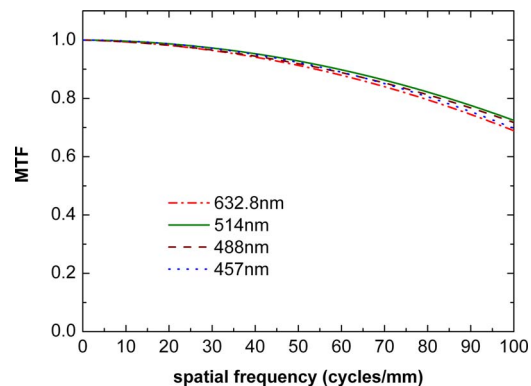


Figure 6. MTF of the scientific camera CCD detector at different wavelengths of the visible spectrum. Curves were determined by fitting experimental values to a second-order polynomial function.

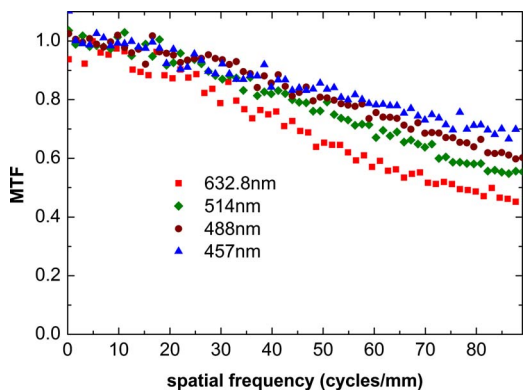


Figure 4. MTF experimental values of the scientific camera CMOS detector at different wavelengths of the visible spectrum.

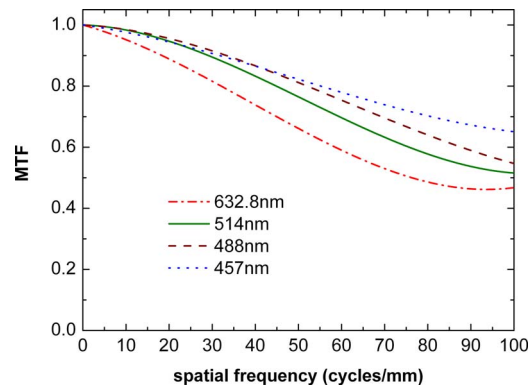


Figure 7. MTF of the scientific camera CMOS detector at different wavelengths of the visible spectrum. Curves were determined by fitting experimental values to a third-order polynomial function.

all the points corresponding to the 512 MTF experimental values are not shown.

In the case of the CCD video camera, given that by definition the MTF is normalized to unity at zero spatial frequency, MTF values higher than 1 are reached due to the amplification introduced by the electronic filters of the image card.^{1,24} Therefore, as the spatial frequency augments, the MTF of the video camera detector first grows until it reaches a maximum value and then begins to degrade with increasing frequency.

Figures 5–7 show, for the three detectors and at the different wavelengths, the MTF curves given by the poly-

mial adjustments of the experimental values after normalization at zero spatial frequency. For each wavelength, the MTF curve of the low-cost video camera CCD detector was determined by fitting experimental values to a third-order polynomial function. The squared correlation coefficients associated with these fits were within the interval from 0.9695 to 0.9916. At the different wavelengths, MTF curves of the scientific camera CCD detector were determined by fitting experimental values to a second-order polynomial function. The squared correlation coefficients corresponding to these

Table II. Experimental MTF maximum values of the video camera CCD detector at different wavelengths: spatial frequencies associated and percentages referring to the highest MTF maximum value.

Wavelength (nm)	Spatial frequency (cycles/mm)	MTF maximum/ MTF maximum at 454 nm (%)
632.8	35.86	68.0
514	38.67	70.2
502	41.85	83.6
488	46.26	91.7
477	43.08	92.2
454	49.44	100.0

adjustments were between 0.9305 and 0.9632. For the scientific camera CMOS detector, MTF curves were determined by fitting experimental values to a third-order polynomial function at each wavelength. The squared correlation coefficients associated with these polynomial fits fell within the range of 0.9598 and 0.9868.

The comparison of the results illustrate the differences between the cameras analyzed with respect to the performance of the MTF of the detector with wavelength, within the spectral range studied. For the detector of the video camera, the differences between the MTF curves corresponding to the different wavelengths analyzed become more noticeable as the spatial frequency increases. Furthermore, the highest value of MTF is reached at the shortest of the wavelengths studied (454 nm), and the MTF decreases as the wavelength increases.

As commented previously, with the CCD video camera, the MTF reaches values higher than unity due to the amplification introduced by the electronic filters of the image card. Related to this fact, our results show that, in general, the value of the spatial frequency for which the maximum of the MTF curve is found increases as the wavelength diminishes. The values of the spatial frequency associated with the experimental MTF maximum values of the video camera are listed in Table II, for all the wavelengths analyzed in this work. Table II also reports the ratio between each experimental MTF maximum value and the highest of them, which corresponds to 454 nm, as observed above.

In summary, the results for the low-cost video camera CCD detector show that the MTF diminishes as the wavelength augments, and that the higher the wavelength, the lower the spatial frequency at which the MTF degradation begins.

For both scientific detectors, the MTF spectral behavior does not show the same trend. Within the range of the visible spectrum, between 457 and 514 nm, no significant differences were apparent in the MTF curves of the scientific detectors resulting at the different wavelengths, at least for spatial frequencies distant from the Nyquist frequency, as stated in previous works.^{25,26}

The overall MTF behavior of the scientific detectors is determined by the geometrical shape of the active pixel area

and the physical-diffusion effect.^{1,27} The effect of the shape of the active pixel area on the overall MTF is especially important for CMOS array detectors, where the fill factor is less than 100%, in contrast to CCD devices, where it can approach this maximum value.²⁷ The diffusion component of the MTF is due to the penetration depth of photons into the substrates and, as the wavelength increases, photon absorption occurs at increasing depths in the detector material.^{1,27} It was therefore expected that the MTF of the scientific detectors should change more at longer wavelengths than as reported in previous research. Accordingly in the present work we are interested in extending the study of the MTF spectral variation of the different detector arrays at higher wavelengths within the visible spectrum.

The new measurements carried out show that, for the scientific CMOS detector, the differences between the MTF curves corresponding to the different wavelength augment with the spatial frequency, as observed for the video camera, too. Specifically, the MTF decreases as the wavelength increases for the spatial frequencies beyond the middle of the interval analyzed (that is, approximately from half of the Nyquist frequency of the detector).

Within the whole spectral range studied here, the MTF spectral behavior of the scientific detectors does not show the same trend, the differences between the MTF curves at the different wavelengths being more notable for the CMOS than for the CCD scientific detector. Even the differences between the MTF curves corresponding to extreme wavelengths are probably not significant for the scientific CCD, as opposed to what appears for the CMOS detector.

Differences in the MTF spectral behavior of the detector arrays studied could be due to the effect of charge diffusion between pixels, which depends on wavelength.¹ Probably, the charge diffusion effect is slightest for the CCD scientific camera, and therefore the wavelength does not influence the MTF of its detector significantly. Besides, in the case of the video camera, the horizontal MTF is also affected by the electronic filters of the image card^{11,24} and, in the case of the CMOS detector, the MTF is influenced by the lower value of the fill factor, too.²⁷ Our results show that the CCD detector yielded MTF values higher than those of the CMOS detector at the same spatial frequencies, for each of the four visible wavelengths analyzed.

CONCLUSIONS

In this work, we have comparatively analyzed the quality of the images provided by different detector arrays in terms of MTF using the speckle method. In addition, we have compared the arrays' performance with wavelength over a range of the visible spectrum. Accordingly, we have studied the MTF at several visible wavelengths, for the detectors of a low-cost CCD video camera and of two scientific cameras (CCD and CMOS).

With the CCD video camera, the MTF reached values higher than one due to the amplification introduced by the electronic filters of the image card. For the CMOS detector, the MTF is also influenced by the lower fill factor.

For all the wavelengths studied, the scientific CCD detector exhibited MTF values higher than those of the CMOS detector.

Moreover, our results reveal differences in the MTF spectral variation of the detector arrays analyzed within the spectral range studied. In the case of the CCD detector of the video camera, the highest value of the MTF was reached at the shortest of the wavelengths studied.

For both the low-cost CCD and the scientific CMOS detectors, differences between the MTF curves become apparent as the spatial frequency augments. Beyond one half of the Nyquist frequency of these detectors, the MTF decreases as the wavelength increases.

In the case of scientific cameras, the MTF spectral behavior does not show the same trend within the spectral range studied, the differences between the MTF curves being more notable for the CMOS detector. For the scientific CCD detector, the differences between the MTF curves corresponding to extreme wavelengths are not likely to be significant; but they are for the scientific CMOS detector.

Since the penetration depth of photons in the detector material increases with the wavelength, effects of smear and signal loss are more pronounced at higher wavelengths. Therefore, the influence of the diffusion on the MTF of the detector is stronger as the wavelength increases.

The new measurements incorporated into the present work demonstrate this fact, as the results found for the scientific CMOS detector and for the CCD detector of the low-cost video camera illustrate. In the cases of the scientific CCD detector, to observe these effects, it would be necessary to carry out new measurements at higher wavelengths than those analyzed here.

In this sense, it is worthwhile to become aware of the differences reported in the MTF spectral behavior of the detector arrays analyzed in our work, taking them into account when choosing a solid-state camera for specific applications within the spectral range we have studied.

ACKNOWLEDGMENTS

The authors express their appreciation to the Ministerio de Educación y Ciencia of Spain for financing projects FIS2004-06465-C02-02 and FIS2007-66671-C02-02.

REFERENCES

- ¹G. C. Holst and T. S. Lomheim, *CMOS/CCD Sensors and Camera Systems* (JCD Publishing, Winter Park, FL and SPIE Optical Engineering Press, Bellingham, WA, 2007).
- ²H. Helmers and M. Schellenberg, "CMOS vs. CCD sensors in speckle interferometry", *Opt. Laser Technol.* **35**, 587–595 (2003).
- ³D. Litwiller, "CCD vs. CMOS: Facts and fiction", *Photonics Spectra* **35**, 154–158 (2001).
- ⁴J. Janesick, "Dueling detectors. CMOS or CCD?", *OE Mag.* **41**, 30–33 (2002).
- ⁵J. Janesick, "Lux transfer: complementary metal oxide semiconductors versus charge-coupled devices", *Opt. Eng.* **41**, 1203–1215 (2002).
- ⁶G. Deptuch, A. Besson, P. Rehak, M. Szeleznik, J. Wall, M. Winter, and Y. Zhu, "Direct electron imaging in electron microscopy with monolithic active pixel sensors", *Ultramicroscopy* **107**, 674–684 (2007).
- ⁷S. K. Park, R. Schowengerdt, and M. Kaczynski, "Modulation-transfer-function analysis for sampled image system", *Appl. Opt.* **23**, 2572–2582 (1984).
- ⁸J. C. Feltz and M. A. Karim, "Modulation transfer function of charge-coupled devices", *Appl. Opt.* **29**, 717–722 (1990).
- ⁹D. N. Sitter, Jr., J. S. Goddard, and R. K. Ferrell, "Method for the measurement of the modulation transfer function of sampled imaging systems from bar-target patterns", *Appl. Opt.* **34**, 746–751 (1995).
- ¹⁰A. Daniels, G. D. Boreman, A. D. Ducharme, and E. Sapir, "Random transparency targets for modulation transfer function measurement in the visible and infrared regions", *Opt. Eng.* **34**, 860–868 (1995).
- ¹¹S. M. Backman, A. J. Makynen, T. T. Kolehmainen, and K. M. Ojala, "Random target method for fast MTF inspection", *Opt. Express* **12**, 2610–2615 (2004).
- ¹²N. Guérineau, J. Primot, M. Tauvy, and M. Caes, "Modulation transfer function measurement of an infrared focal plane array by use of the self-imaging property of a canted periodic target", *Appl. Opt.* **38**, 631–637 (1999).
- ¹³M. Marchywka and D. G. Socker, "Modulation transfer function measurement techniques for small-pixel detectors", *Appl. Opt.* **31**, 7198–7213 (1992).
- ¹⁴J. E. Greivenkamp and A. E. Lowman, "Modulation transfer function measurements of sparse-array sensors using a self-calibrating fringe pattern", *Appl. Opt.* **33**, 5029–5036 (1994).
- ¹⁵A. M. Pozo, A. Ferrero, M. Rubiño, J. Campos, and A. Pons, "Improvements for determining the modulation transfer function of charge-coupled devices by the speckle method", *Opt. Express* **14**, 5928–5936 (2006).
- ¹⁶G. D. Boreman and E. L. Dereniak, "Method for measuring modulation transfer function of charge-coupled devices using laser speckle", *Opt. Eng.* **25**, 148–150 (1986).
- ¹⁷A. D. Ducharme, "Microlens diffusers for efficient laser speckle generation", *Opt. Express* **15**, 14573–14579 (2007).
- ¹⁸G. D. Boreman, Y. Sun, and A. B. James, "Generation of laser speckle with an integrating sphere", *Opt. Eng.* **29**, 339–342 (1990).
- ¹⁹M. Sensiper, G. D. Boreman, A. D. Ducharme, and D. R. Snyder, "Modulation transfer function testing of detector arrays using narrow-band laser speckle", *Opt. Eng.* **32**, 395–400 (1993).
- ²⁰A. M. Pozo and M. Rubiño, "Comparative analysis of techniques for measuring the modulation transfer functions of charge-coupled devices based on the generation of laser speckle", *Appl. Opt.* **44**, 1543–1547 (2005).
- ²¹J. W. Goodman, "Laser Speckle and Related Phenomena", edited by J. C. Dainty, *Topics in Applied Physics*, Vol. **9** (Springer-Verlag, Berlin, 1984) pp. 35–40.
- ²²L. I. Goldfisher, "Autocorrelation function and power spectral density of laser-produced speckle patterns", *J. Opt. Soc. Am.* **55**, 247–253 (1965).
- ²³G. D. Boreman, "Fourier spectrum techniques for characterization of spatial noise in imaging arrays", *Opt. Eng.* **26**, 985–991 (1987).
- ²⁴B. T. Teipen and D. L. MacFarlane, "Liquid-crystal-display projector-based modulation transfer function measurements of charge-coupled-device video camera systems", *Appl. Opt.* **39**, 515–525 (2000).
- ²⁵A. Fernández-Oliveras, A. M. Pozo, and M. Rubiño, "Análisis de la variación espectral de la MTF de videocámaras CCD mediante patrones de moteado láser", *Opt. Pura Apl.* **41**, 221–225 (2008).
- ²⁶A. Fernández-Oliveras, A. M. Pozo, and M. Rubiño, "MTF spectral-variation comparison of detector arrays used in multispectral imaging systems by speckle patterns", *Proc. IS&T's 4th European Conference on Colour in Graphics, Imaging, and Vision; 10th International Symposium on Multispectral Colour Science* (IS&T, Springfield, VA, 2008) pp. 461–466.
- ²⁷I. Shcherback and O. Yadid-Pecht, *CMOS Imagers: From Phototransduction to Image Processing*, edited by O. Yadid-Pecht and R. Etienne Cummings (Kluwer Academic, Norwell, MA, 2004) pp. 53–74.